Strontium-substituted calcium magnesium silicate single crystals for high-temperature piezoelectric applications

Hiroaki Takeda, Hiraku Kusakabe, Haruki Usui, Takuya Hoshina, Takaaki Tsurumi, Kheirreddine Lebbou

Journal of the Ceramic Society of Japan 128 [3] 130-134 2020
DOI http://doi.org/10.2109/jcersj2.19193

JCS-Japan

FULL PAPER

Strontium-substituted calcium magnesium silicate single crystals for high-temperature piezoelectric applications

Hiroaki TAKEDA[1,†], Hiraku KUSAKABE[1], Haruki USUI[1], Takuya HOSHINA[1], Takaaki TSURUMI[1] and Kheirreddine LEBBOU[2]

[1]School of Materials and Chemical Technology, Tokyo Institute of Technology, Meguro, Tokyo 152–8552, Japan
[2]Institut Lumière Matière, UMR5306 CNRS, Universite de Lyon 1, 69622 Villeurbanne Cedex, France

We present a relationship between piezoelectric property and crystal structure in melilite-type crystals. Two independent piezoelectric constants, d_{14} and d_{36}, increase and decrease with the polyhedral distortion, respectively. Based on this knowledge, single crystals made of strontium-substituted calcium magnesium silicate $Ca_2MgSi_2O_7$ (CMS) have been submitted to the Czochralski method, which made them grown. The CMS crystal has a high d_{36}; however, its transition temperature is around 85 °C. Therefore, the strontium substitution is conducted to decrease this phase transition temperature. A single crystal of strontium substituted CMS, with nominal chemical composition $Ca_{1.7}Sr_{0.3}MgSi_2O_7$ (CSMS30), shows no phase transition when temperature rises from room to melting temperature. Its piezoelectric d'_{31} constant is 2.1 pC/N and its compressive strength is 830 MPa on crystal substrate with (*ZXt*)45° cut. The CSMS30 single crystal is a superior candidate material for pressure sensors at high operating temperatures.

Key-words : Silicate, Crystal growth, Piezoelectricity, High temperature

[Received October 24, 2019; Accepted January 12, 2020]

1. Introduction

High-temperature piezoelectric crystals are still highly demanded due to their potential applications, such as gas sensors, gas injectors, and combustion pressure sensors (CPS). Among them, the CPS application is the one which the special features of piezoelectric materials are more demanded and the following five conditions need to be satisfied: (i) no phase transitions (thermal stability of piezoelectric properties); (ii) neglectable pyroelectric properties (only piezoelectric response is produced); (iii) high resistivity (even at elevated temperatures) for long-term charge holding; (iv) high mechanical strength for high-pressure conditions; and (v) easy to be synthesized for suitable mass production.

As the promising candidates for high-temperature use, langasite $La_3Ga_5SiO_{14}$ (LGS)-type crystals,[1),2)] rare-earth calcium oxoborate $ReCa_4O(BO_3)_3$ (Re = rare earth elements, *Re*COB) crystals,[3)] gallium phosphate $GaPO_4$,[4)] and AlN, as well as its modified crystal[5)] or thick films[6)–8)] have been investigated during the last two decades. In the past decade, $Ba_2TiSi_2O_8$,[9)] α-$Ba_2TeMo_2O_9$,[10)] $Bi_4Ti_3O_{12}$,[11)] α-BiB_3O_6[12)] and melilite-type crystals, such as $Ca_2Al_2SiO_7$ (CAS)[13)] and $SrLaGa_3O_7$[14)] have been reported as promising materials. These crystals, however, do not satisfy all the conditions listed. CPS made of langasite-type crystals has been attempted to be developed for practical applications until now.

The CAS crystal does not satisfy the condition (iv) of our survey prior to this study. Melilite-type crystals belong to the tetragonal $P\bar{4}2_1m$ space group. A crystal with $P\bar{4}2_1m$ symmetry has two independent piezoelectric constants (d_{14} and d_{36}) in shear mode. On the other hand, in compression mode, piezoelectric responses can also be obtained from using crystal substrates with both $(XYt)\theta°$ and $(ZXt)\theta°$ rotation cuts, respectively.[15),16)] As d_{14} is always higher than d_{36} with respect to crystals, compressive strength of the $(XYt)45°$ cut, showing the highest d_{14} value in the CAS crystal, was measured in our previous study.[17)] The compressive strength of 140 MPa is, however, insufficient for practical applications. This low strength is achieved because the melilite-type crystals have a distinct cleavage plane, which is normal to the crystallographic *c*-axis, which corresponds to the crystallographic {001} plane. This cleavage plane agrees with the direction of shearing stress on the $(XYt)45°$ cut, causing low mechanical strength.

A possible way to find another candidate is to focus on d_{36} on the $(ZXt)45°$ cut. Single crystals of calcium magnesium silicate $Ca_2MgSi_2O_7$ (CMS), also known as the mineral akermanite, are grown from a melt with stoichiometric composition by employing the Czochralski (Cz) method.[18),19)] The CMS crystal shows high d_{36}, above

† Corresponding author: H. Takeda; E-mail: htakeda@ceram.titech.ac.jp

4 pC/N,[19] however, a commensurate-incommensurate phase transition occurs around 85 °C,[20] when the d_{36} value drops. Although the strontium substitution into CMS decrease the phase transition's temperature,[21] no report about substitution effect on piezoelectric property have been conducted. Moreover, a relationship between the piezoelectric property and crystal structure may indicate how strontium substitution affects this property of the melilite-type crystals.

In this paper, we first report a relationship between piezoelectric property and crystals' structure in melilite-type crystals. Phase transition temperature change is presented using Sr-substituted CMS crystal powders. We demonstrate the material's applicability to high-temperature piezoelectric sensors by showing the sufficient piezoelectric property and mechanical strength of Sr-substituted CMS single crystals grown with the Cz method.

2. Experimental

The data of piezoelectric property and structural parameters of melilite-type crystals was collected.[14),19),22)–28)] Crystal growth experiments were conducted using both the Cz and the laser-heated pedestal growth (LHPG) methods.[29)] Prior to the Cz method, the LHPG method was applied as it is able to determine their optimum compositions for bulk growth. The growth speed and atmosphere were 0.3 mm/min and air, respectively and the detailed process is described in the Refs. 17), 29). Stoichiometric amounts of oxides and carbonates with 99.99% purity, corresponding to $Ca_{2-x}Sr_xMgSi_2O_7$ ($x = 0.00$–0.6: CSMS100x), were prepared and calcined at 1350–1390 °C for 4 h in air. We, afterwards, shaped the ceramics into rods, which were used as charge and seed rods for the LHPG method, with dimensions of 1.0 × 1.0 × 30–40 mm. The as-grown crystals were polished, and their chemical composition was, afterwards, determined by electron probe micro analyzer. The crystals were also pulverized, and used for differential scanning calorimetry (DSC) measurement.

Based on the LHPG growth's results, CSMS10 and CSMS30 single crystals were grown by the Cz method. Single crystals were also grown with a conventional RF-heating Cz technique, using an iridium crucible (50 mm in diameter and height). The raw materials were the same powders as those used for the LHPG method. They were mixed in air, calcined at 1350 °C, and charged into the crucible. The growth atmosphere with low oxygen partial pressure was achieved by flowing an argon gas at 10^{-3} m^3/min. The initial seed for CSMS10 was a CMS ceramic bar. The grown CSMS10 crystal was cut along *a*-axis after orientation determination using a back scattering Laue X-ray diffraction and used as the seed crystal for further growth. The pulling rate and the rotation rate were 1.0 mm/h and 10 rpm, respectively. Phase identification of the as-grown crystals was performed by powder XRD, and the crystal density was calculated using lattice parameter and chemical composition.

The electric resistivity ρ at room temperature was measured. Electroacoustical constants (the dielectric, piezoelectric, and elastic compliance constants) of single crystals made of CSMS10 and CSMS30 were determined with Agilent 4294A Impedance/Gain Phase Analyzer as indicated in Refs. 15), 16), 30). We fabricated equivalent (*ZXt*)45° cut plate resonators with dimensions of 12 × 3 × 0.8 mm. This study is focused on the piezoelectric constant d'_{31} expressed by the equation $d'_{31} = d_{36} \sin 2\theta/2$ using the piezoelectric modulus d_{36} and the rotation angle θ. Furthermore, d'_{31} was evaluated by measuring resonant and anti-resonant frequencies of the resonators in the length-extensional mode. Moreover, the temperature dependences of the CAS crystals' d'_{31} were compared to those of the langasite family crystals [$Ca_3TaAl_3Si_2O_{14}$ (CTAS),[1)] $Ca_3TaGa_3Si_2O_{14}$ (CTGS),[1)] LGS,[31)] $La_3Ta_{0.5}Ga_{5.5}O_{14}$ (LTG),[31)] and Al-doped LTG (LTGA)[2),31)]] and $YCa_4O(BO_3)_3$(YCOB) crystal.[3)]

Compression tests were conducted as reported in Ref. 17) to determine the compressive strength of the crystal substrates with a compression tester (Shimazu EZ-LX). In this study, the procedures were set according to JIS R1608.[32)] 20 samples of (*ZXt*)45° cut were fabricated in the form of rectangular parallelepipeds with dimensions of 1 × 1 × 2.5 mm. The load speed was 1 mm/min. We compared the compressive strength of the (*ZXt*)45° cut of the CSMS30 crystal and that of the (*XYt*)45° of the CAS crystals.

3. Results and discussion

In the melilite-type crystal structure, three types of cation sites exist and the chemical formula can be represented as $A_2(T1)(T2)_2O_7$, where the notation *A* represents 8-coordinated sites and T1 and T2 represent crystallographically independent tetrahedral sites as shown in **Fig. 1**. In our previous report,[23)] the piezoelectric constant d_{14} and the polyhedral distortion Δ for the 8-coordinated *A* site of CAS crystal are reduced by Sr-substitution. Δ is defined as $\Delta = (1/N)\sum_i\left[(R_i - \bar{R})/\bar{R}\right]^2$, where *N* is the coordination number, R_i is the individual bond length, and $\bar{R}$ is the average bond length.[33)] The report indicates how to find a relationship between piezoelectric property and crystal structure in melilite-type crystals.

Figure 2 shows the piezoelectric constants, d_{14} and d_{36}, versus the polyhedral distortion Δ for the *A* site. d_{14} increases with Δ, on the other hand, d_{36} slightly decreases.

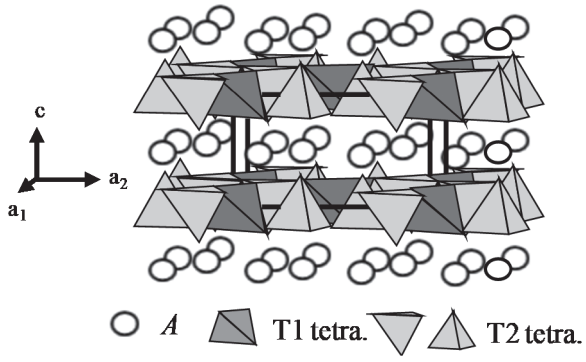

Fig. 1. A schematic crystal structure of melilite.

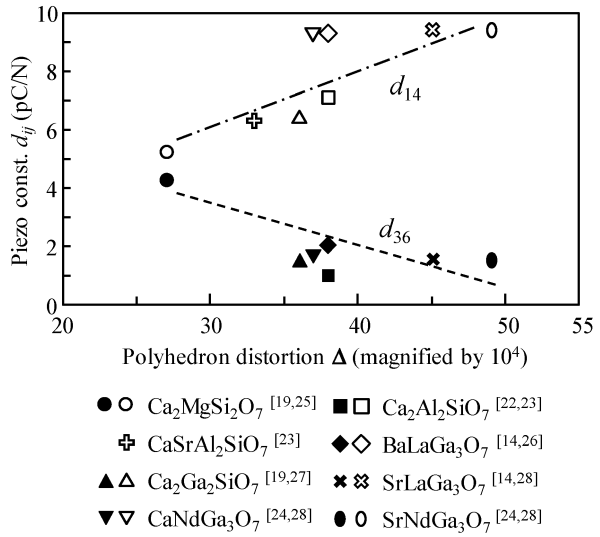

Fig. 2. Piezoelectric constants, d_{14} and d_{36}, versus the structural distortion Δ of the A site in melilite-type crystals. The numbers in superscript square brackets following the chemical formula correspond to those indexed in the references.

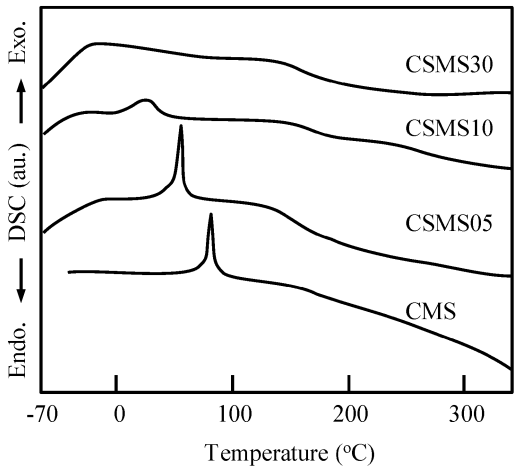

Fig. 3. DSC curves for $Ca_{2-x}Sr_xMgSi_2O_7$ crystals with $x = 0.0$, 0.05, 0.10, and 0.30, abbreviated as CMS, CSMS05, CSMS10, CSMS30, respectively. The data was collected during cooling process.

Table 1. Mass density, Electromechanical coupling factor and materials constants of $(Ca_{2-x}Sr_x)MgSi_2O_7$ crystal with $x = 0.30$ (CSMS30), measured at room temperature (25 °C)

Crystal density[a] [g/cm^3]	D_x	3.06
Electromechanical coupling factors	k'_{31}[b]	0.10
Elastic compliance constant [10^{-12} m^2/N]	s_{33}^E	6.71
Piezoelectric constants [pC/N]	d'_{31}[b]	2.11
	d_{36}	4.22
Relative dielectric constant [—]	$\varepsilon_{33}^T/\varepsilon_0$	7.60

[a]Calculated density using lattice parameters and chemical composition. [b]Vibration mode: Length-extensional (transverse effect), crtstal substrate: (*ZXt*)45° cut.

The reason for that behavior is still under investigation by using Ab initio calculation. This study is focused on the piezoelectric d'_{31} constant, originated from d_{36}, as the (*XYt*)45° cut showing d'_{31}, originated from d_{14}, has low mechanical strength. Moreover, d'_{31} should be comparable to d_{11} (2.20 pC/N[34]) of quartz crystal, which is usually employed for conventional combustion pressure sensor materials. We have focused, therefore, on the CMS crystal with high d_{36} and modified the crystal by element substitution.

All the grown CSMS100x crystals produced by the LHPG method were composed of melilite-type crystal without any impurity phases. **Fig. 3** shows DSC curves for CMS and Sr-substituted CMS crystals during cooling process. The curves of the CMS and the CSMS05 have a distinct exothermal peak at 82 and 57 °C, respectively. On the other hand, the curve on the CSMS10 has a blunt peak around 24 °C. These temperatures values are in good agreement with reported incommensurate-commensurate (normal) phase transition temperatures,[21] even though no peak was observed on the CSMS30 case. This means that the CSMS30 crystal does not show abrupt change of piezoelectric constant with the elevating temperature, a benefitting feature for applications.

Based on these observations, CSMS10 and CSMS30 single crystals were grown by the Cz method. Both were successfully grown by pulling them along the ⟨100⟩ direction. The single crystals had 18–20 mm in diameter and 40–70 mm in length. The crystals showed a smooth surface and were transparent. No cracks and twins were found under polarized optical microscopic observation.

In the melilite-type crystal with the point group $\bar{4}2m$, the total number of electroacoustical constants is 10, including two dielectric ε_{ij}, two piezoelectric d_{ij}, and six elastic compliance s_{ij} constants. **Table 1** shows the calculated mass density, the electromechanical coupling factor, and some electroacoustical constants of the CSMS30 single crystal. These constants were obtained using (*ZXt*)45° cuts. d'_{31} value is 2.11 pC/N, similar to the d_{11} of quartz crystal (already mentioned). As the d'_{31} constant indicates an electrical charge generated by normal compression stress, the d'_{31} value of the (*ZXt*)45° cut of CSMS30 is applicable to high-temperature pressure sensors. At room temperature, the electric resistivity ρ of the CSMS30 crystal exceeded a measuring limit (over 10^{13} Ω cm at least). Shen et al.[19] reported that the ρ at 250 °C of the CMS crystal is in the 10^{12} Ω cm order while, at room temperature, it could not be measured due to ultrahigh values. In this study, we substituted Ca^{2+} by Sr^{2+} in the CMS crystal. This substitution maintains charge neutrality of the CMS crystal and may slightly affect electronic conduction. As a result, the CSMS crystal should have high electric resistivity, satisfying the condition (iii).

Figure 4 shows the temperature dependence of the piezoelectric constant $d'_{31}(= 1/2\ d_{36})$ obtained at (*ZXt*)45° cut of the CMS and Sr-substituted CMS crystals. The data of CMS are reported in Ref. 19). We determined the d'_{31} by the resonance and anti-resonance method. For this method, it is essential to eliminate the effects of parasitic capacitance; therefore, the coaxial cables were located close to the furnace. On both the CMS and CSMS10 crys-

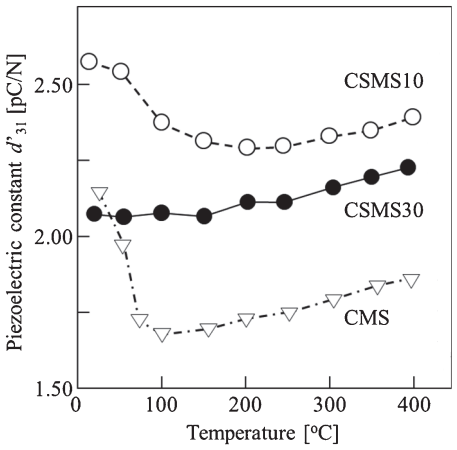

Fig. 4. Piezoelectric d'_{31} constants as a function of temperature for $Ca_{2-x}Sr_xMgSi_2O_7$ crystals with $x = 0.0$, 0.10, and 0.30, abbreviated as CMS, CSMS10, CSMS30, respectively. The data of CMS is referred to that reported in Ref. 19).

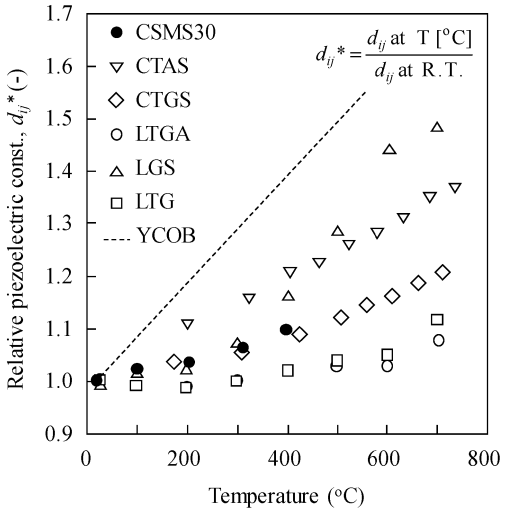

Fig. 5. Relative piezoelectric constants as a function of temperature for $Ca_{2-x}Sr_xMgSi_2O_7$ with $x = 0.30$ (CSMS30) crystals compared with other high-temperature crystals. The abbreviations of the crystals correspond to those in the main text. A dash line of YCOB is calculated using the data reported in Ref. 3).

tals, d'_{31} values dropped approximately when phase transition was reached and increased with temperature. On the other hand, d'_{31} values of the CSMS30 crystal monotonously and slightly increased with temperature.

The temperature dependence of CSMS30 crystal's d'_{31} was compared with d_{11} of other high-temperature piezoelectric crystals,[1)–3),31)] as shown in **Fig. 5**. In this figure, d_{ij}* represents the ratio of the d_{ij} at the measurement temperature and at room temperature (25 °C). d_{11}* values increased with temperature among the langasite family of crystals and the $YCa_4O(BO_3)_3$ crystal presented the largest variation of all crystals. The CSMS30 crystal exhibited a change in d_{ij}* with temperature of about 300 ppm/°C, which is still comparable to that of $La_3Ta_{0.5}Ga_{5.5}O_{14}$ and $La_3Ta_{0.5}Ga_5Al_{0.5}O_{14}$,[35)] (the most promising candidates for CPS nowadays).

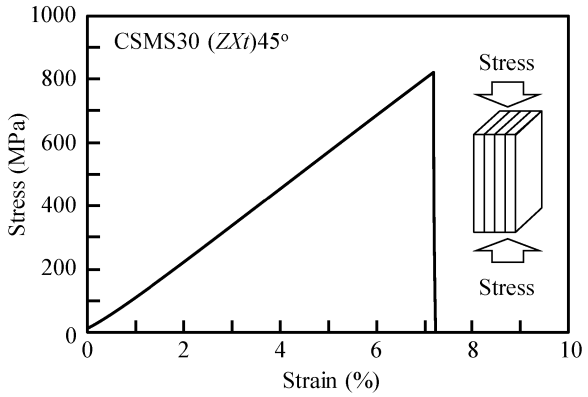

Fig. 6. Typical stress–strain curve for the (*ZXt*)45° cut of CSMS30 crystal. The stripes in the schematic samples correspond to the cleavage plane {001}.

Figure 6 shows the stress–strain curves for the crystal substrate (*ZXt*)45° of CSMS30. The compressive strength of the CSMS30 crystal was 830 MPa, approximately five times higher than that (170 MPa) of the (*XYt*)45° cut of Sr-substituted CAS crysal.[17)] The stress–strain curve before destruction were also similar to the previous report.[17)] The compressive strength of $La_3Ta_{0.5}Ga_{5.5}O_{14}$-based crystals is more than 1000 MPa.[35)] Measurement conditions, such as sample shape, and the load speed in the Ref. 35) were quite different from that in this study, according to JIS R1608.[32)] It was reported that the maximum combustion pressure in a petrol engine is approximately 20 MPa.[36)] Taking this into account, the compressive strength of (*ZXt*)45° cut of the CSMS30 crystal is high enough; therefore, the obtained results suggest that the CSMS30 crystal is a candidate material for manufacturing pressure sensors subjected to high temperatures. Furthermore, CSMS30 crystals are composed of more common elements (Ca, Mg, Sr and Si) when compared to $La_3Ta_{0.5}Ga_{5.5}O_{14}$-based crystals. The CSMS30 crystals can be, therefore, widely used in various piezoelectric devices under high-temperature conditions.

4. Conclusion

We found that two independent piezoelectric constants, d_{14} and d_{36}, in the melilite-type crystal increase and decrease with polyhedral distortion, respectively. The crystal growth of Sr-substituted CMS was, therefore, performed by using the LHPG and Cz methods. The $Ca_{1.9}Sr_{0.1}MgSi_2O_7$ (CSMS10) and $Ca_{1.7}Sr_{0.3}MgSi_2O_7$ (CSMS30) single crystals were successfully grown. CSMS30, in particular, shows no phase transition up to its melting temperature, the piezoelectric property comparable to that of quartz, and high compressive strength are sufficient values for application scenarios. As these findings succeeded in overcoming the shortages of the melilite-type crystals, CSMS30 is able to become an attractive candidate for pressure sensor applications at elevated temperatures.

Acknowledgments We would like to thank Professor T. Ikoma of Tokyo Institute of Technology for helpful sugges-

tions regarding DSC measurements. Parts of this study were financially supported by the Grants-in-Aid for Scientific Research program of the Japan Society for the Promotion of Science (JSPS KAKENHI, grant number 19H02797) and Izumi Science and Technology Foundation.

References

1) S. Zhang, Y. Zheng, H. Kong, J. Xin, E. Frantz and T. R. Shrout, *J. Appl. Phys.*, 105, 114107 (2009).
2) S. Zhang, A. Yoshikawa, K. Kamada, E. Frantz, R. Xia, D. W. Snyder, T. Fukuda and T. R. Shrout, *Solid State Commun.*, 148, 213–216 (2008).
3) F. Yu, S. Zhang, X. Zhao, D. Yuan, L. Qin, Q. M. Wang and T. R. Shrout, *IEEE Trans. Ultrason. Ferroelectr. Freq. Control*, 58, 868–873 (2011).
4) P. Krempl, G. Schleinzer and W. Wallnöfer, *Sensor. Actuat. A-Phys.*, 61, 361–363 (1997).
5) Y. Ooishi, K. Kishi, M. Akiyama, H. Noma, T. Tabaru and D. Nishijima, *J. Ceram. Soc. Jpn.*, 114, 657–659 (2005) [in Japanese].
6) M. Akiyama, T. Kamohara, K. Kano, A. Teshigahara, Y. Takeuchi and N. Kawahara, *Adv. Mater.*, 21, 593–596 (2009).
7) M. Bickermann, B. M. Epelbaum, O. Filip, B. Tautz, P. Heimann and A. Winnacker, *Phys. Status Solidi C*, 9, 449–452 (2012).
8) R. Radhakrishnan Sumathi, *CrystEngComm*, 15, 2232–2240 (2013).
9) C. Shen, H. Zhang, H. Cong, H. Yu, J. Wang and S. Zhang, *J. Appl. Phys.*, 116, 044106 (2014).
10) Z. Gao, X. Tian, J. Zhang, Q. Wu, Q. Lu and X. Tao, *Cryst. Growth Des.*, 15, 759–763 (2015).
11) Y. Kitanaka, Y. Noguchi, M. Miyayama and Y. Kagawa, *Jpn. J. Appl. Phys.*, 51, 09LD08 (2012).
12) F. Chen, L. Kong, F. Yu, C. Wang, Q. Lu, S. Zhang, Y. Li, X. Duan, L. Qin and X. Zhao, *CrystEngComm*, 19, 546–551 (2017).
13) H. Takeda, M. Hagiwara, H. Noguchi, T. Hoshina, T. Takahashi, N. Kodama and T. Tsurumi, *Appl. Phys. Lett.*, 102, 242907 (2013).
14) C. Shen, Y. Zhang, H. Yu, S. Zhang, W. Cao, J. Wang and H. Zhang, *J. Alloy. Compd.*, 647, 1069–1074 (2015).
15) W. P. Mason, "Piezoelectric Crystals, Their Application to Ultrasonics", D. Van. Nostrand, New York (1950).
16) T. Ikeda, "Fundamentals of Piezoelectricity", Oxford Science, Oxford (1990).
17) T. Oshima, T. Hoshina, T. Tsurumi, K. Lebbou and H. Takeda, *J. Ceram. Soc. Jpn.*, 126, 300–305 (2018).
18) C. B. Finch, G. W. Clark, L. A. Harris and C. S. Yust, *J. Cryst. Growth*, 23, 295–298 (1974).
19) C. Shen, S. Zhang, W. Cao, J. Wang, H. Cong, H. Yu and H. Zhang, *J. Appl. Phys.*, 117, 064106 (2015).
20) B. S. Hemingway, H. T. Evans, G. L. Nord, H. T. Haselton, R. A. Robie and J. J. McGee, *Can. Mineral.*, 24, 425–434 (1986).
21) H. Rager, M. Schosnig, A. K. Schaper, A. Kutoglu and W. Treutmann, *Z. Krist.*, 215, 495–498 (2000).
22) H. Takeda, K. Akimoto, T. Oshima, K. Takizawa, J. Kondoh, A. Matsutani, T. Hoshina and T. Tsurumi, *Jpn. J. Appl. Phys.*, 57, 11UD01 (2018).
23) H. Takeda, K. Yoshida, H. Okudera, K. Lebbou, T. Hoshina and T. Tsurumi, *J. Ceram. Soc. Jpn.*, 125, 23–26 (2017).
24) C. Shen, S. Zhang, D. Wang, T. Xu, W. Cao, J. Wang, H. Yu and H. Zhang, *CrystEngComm*, 17, 1791–1799 (2015).
25) M. Hamada and M. Akasaka, *Phys. Chem. Miner.*, 40, 259–270 (2013).
26) J. Hanuza, K. Hermanowicz, M. Maczka, W. Ryba-Romanowski, T. Lis and M. Berkowski, *J. Raman Spectrosc.*, 26, 255–263 (1995).
27) A. A. Kaminskii, E. L. Belokoneva, B. V. Mill, S. E. Sarkisov and K. Kurbanov, *Phys. Status Solidi A*, 97, 279–290 (1986).
28) J. M. S. Skakle and R. Herd, *Powder Diffr.*, 14, 195–202 (1999).
29) K. Lebbou and G. Boulon, "Fiber Crystal Growth from the Melt, Advances in Materials Research", Ed. by T. Fukuda, P. Rudolph and S. Uda, Springer-Verlag, Berlin (2004) pp. 219–254.
30) IEEE Standard on Piezoelectricity, "IEEE Standard on Piezoelectricity", ANSI/IEEE Std 176 (1987).
31) H. Takeda, J. Yamaura, T. Nishida, T. Hoshina and T. Tsurumi, *Cryst. Res. Technol.*, 50, 944–949 (2015).
32) JIS R1608: 2003. Testing methods for compressive strength of fine ceramics.
33) R. D. Shannon, *Acta Crystallogr. A*, 32, 751–766 (1976).
34) "Piezoelectric single crystals and their applications", Ed. by S. Trolier-McKinstry, L. E. Cross and Y. Yamashita, Pennsylvania State University, University Park, PA (2004).
35) I. Takahashi, T. Aoki, Y. Nonogaki and Y. Kinoshita, Japan patent WO2017030166 (2017).
36) K. Tsukada, M. Takeuchi, S. Tokumitsu, Y. Ohmura and K. Kawaguchi, *R&D Rev. Toyota CRDL*, 28, 49–56 (1993) [in Japanese].